Pharmaceutical Research, Vol. 26, No. 3, March 2009 (© 2008)
DOI: 10.1007/s11095-008-9760-7

Research Paper

Polymer Chemistry Influences Monocytic Uptake of Polyanhydride Nanospheres

Bret D. Ulery,[1] Yashdeep Phanse,[2] Avanti Sinha,[2] Michael J. Wannemuehler,[2] Balaji Narasimhan,[1,3] and Bryan H. Bellaire[2,3]

Received September 7, 2008; accepted October 14, 2008; published online November 6, 2008

Purpose. To demonstrate that polyanhydride copolymer chemistry affects the uptake and intracellular compartmentalization of nanospheres by THP-1 human monocytic cells.
Methods. Polyanhydride nanospheres were prepared by an anti-solvent nanoprecipitation technique. Morphology and particle diameter were confirmed via scanning election microscopy and quasi-elastic light scattering, respectively. The effects of varying polymer chemistry on nanosphere and fluorescently labeled protein uptake by THP-1 cells were monitored by laser scanning confocal microscopy.
Results. Polyanhydride nanoparticles composed of poly(sebacic anhydride) (SA), and 20:80 and 50:50 copolymers of 1,6-bis-(*p*-carboxyphenoxy)hexane (CPH) anhydride and SA were fabricated with similar spherical morphology and particle diameter (200 to 800 nm). Exposure of the nanospheres to THP-1 monocytes showed that poly(SA) and 20:80 CPH:SA nanospheres were readily internalized whereas 50:50 CPH:SA nanospheres had limited uptake. The chemistries also differentially enhanced the uptake of a red fluorescent protein-labeled antigen.
Conclusions. Nanosphere and antigen uptake by monocytes can be directly correlated to the chemistry of the nanosphere. These results demonstrate the importance of choosing polyanhydride chemistries that facilitate enhanced interactions with antigen presenting cells that are necessary in the initiation of efficacious immune responses.

KEY WORDS: adjuvants; antigen presenting cells; chemistry; immune response; polyanhydride.

INTRODUCTION

Bioerodible polymers have been studied as sustainable drug delivery vehicles for over thirty years (1). Polyesters and polyanhydrides are two families of polymers that are strong candidates for biomedical applications because of the biocompatibility and bioresorbability of their degradation products (2). While polyesters, like poly(lactic-*co*-glycolic acid) (PLGA), have been approved by the FDA for many *in vivo* applications (3), their suitability for use as vaccine delivery vehicles is affected by various factors that negatively impact the stability of encapsulated proteins. Research has shown that the bulk-erodible polyester-based delivery systems display rapid release profiles (4,5), produce low pH microenvironments (6–8), and can initiate moisture-induced protein aggregation (8–10). In contrast, polyanhydrides are characterized by chemistry-dependent surface erosion and payload release (11–13), moderate pH microenvironments (8,14,15), and superior protein stabilization capabilities (10,16,17). Polyanhydrides have been used to deliver plasmid DNA (18), proteins (9,13,17), small molecular weight drugs (11,19,20), and vaccine immunogens (21,22). Alterations of polyanhydride chemistry modulate degradation rates from weeks to years, which can be exploited to best fit therapeutic needs (9,11,16). In addition, polyanhydride microspheres used as vaccine delivery vehicles exhibit a chemistry-dependent, immunomodulatory adjuvant effect (22). Kipper *et al.* showed that encapsulating tetanus toxoid (TT) into polyanhydride microspheres or co-delivering free TT along with the microspheres enhanced antigen-specific immune responses (22). Furthermore, the relative increase of polymer hydrophobicity effectively modulated the immune response from a dominant T_H2 (humoral) to a T_H0 (balanced) response. Together, these results indicate that polyanhydride microspheres are promising vehicles for vaccine delivery.

The polyanhydride chemistries used in the present study were copolymers of sebacic anhydride (SA) and 1,6-bis-(*p*-carboxyphenoxy)hexane (CPH) anhydride with chemical structures as shown in Fig. 1. With aromatic rings, the CPH unit is more hydrophobic than the aliphatic SA unit. Copolymers containing higher compositions of CPH have been shown to degrade slower than copolymers containing higher compositions of SA (9).

In the last several decades, the *in vivo* applications utilizing polymer carriers have transitioned from the use of large, implanted pellets (~1 mm) to microspheres (~5–20 μm) and, more recently, to nanospheres (~100–500 nm) (1,11). In comparison to implants, microspheres (or nanospheres) do not require surgical insertion or removal (22), can

[1] Department of Chemical and Biological Engineering, Iowa State University, Ames, IOWA 50011, USA.
[2] Department of Veterinary Microbiology and Preventive Medicine, Iowa State University, Ames, IOWA 50011, USA.
[3] To whom correspondence should be addressed. (e-mail: nbalaji@iastate.edu)

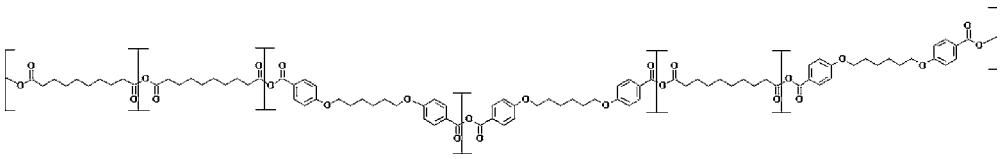

Fig. 1. Chemical structure of a random CPH:SA copolymer.

carry multiple drugs (20,23), and are phagocytosed by antigen presenting cells (APCs) (24). Inhalation and intranasal delivery can be realized with particles that are small enough to pass through the finely porous networks of the nasal, tracheal, and pulmonary filtration systems (25,26). In addition, multiple studies have shown that polymeric nanoparticles gain ready access into sub-mucosal layers of the nasal-associated and gut-associated lymphoid tissues much more effectively than microparticles (27–29). In comparison to microspheres, nanospheres were more readily taken up by APCs (30). Collectively, these characteristics underpin the functional diversity and enhanced capabilities of polyanhydride nanospheres.

In order for polyanhydride nanospheres to function as efficacious vaccine adjuvants, they must possess the ability to stimulate and to deliver antigen to APCs. In the present study, we chose to use confocal microscopy to monitor both intracellular and extracellular interactions between polyanhydride nanospheres and APCs (31). In addition, confocal microscopy allowed us to monitor the potential for polyanhydride nanospheres to deliver antigen via the endocytic pathway by evaluating the co-localization of polyanhydride nanospheres within specific sub-cellular compartments associated with antigen processing and presentation. Our data demonstrate that systematically varying the chemistry of polyanhydride nanospheres (by varying the SA content in a CPH:SA copolymer) significantly affects nanosphere uptake by human monocytic cells. In addition, we demonstrate that polymer chemistry significantly influences the uptake of a model antigen (Eα tagged with red fluorescent protein (RFP), henceforth referred to as Eα-RFP) by human monocytic cells.

MATERIALS AND METHODS

Materials

Sebacic acid (99%), 4-hydroxybenzoic acid, 1-methyl-2-pyrrolidinone anhydrous (99.5%), 1,6-dibromohexane (98.5%) and fluorescein-isothiocyanate-dextran (FITC-dextran) were purchased from Sigma-Aldrich (Milwaukee, WI, USA). All other chemicals were purchased from Fisher Scientific (Pittsburgh, PA, USA) and used as received.

Polyanhydride Synthesis and Characterization

Synthesis of SA and CPH pre-polymers and copolymers was performed as previously described (11,12,32). The resulting polymers were characterized using ^{1}H nuclear magnetic resonance to verify polymer chemistry, gel permeation chromatography to analyze molecular weight, and differential scanning calorimetry to determine glass transition temperature and crystallinity. All properties evaluated showed that the synthesized polymers were within accepted ranges (11,12).

Nanosphere Fabrication and Characterization

FITC-dextran loaded nanospheres were fabricated by polyanhydride anti-solvent nanoencapsulation (PAN), similar to the method reported by Mathiowitz *et al.* for poly (fumaric acid-co-sebacic acid) polymers (33). Polymer (145.5 mg) was dissolved in methylene chloride (5 mL) held at room temperature for poly(SA) and 20:80 CPH:SA and 0°C for 50:50 CPH:SA. FITC-dextran (4.5 mg) was added to the polymer solution and homogenized at 30,000 rpm for 30 s to create a suspension. The polymer/fluorescein solution was rapidly poured into a bath of petroleum ether at an anti-solvent to solvent ratio of 80:1 held at room temperature for poly(SA) and 20:80 CPH:SA and -40°C for 50:50 CPH:SA (due to the lower glass transition temperature for 50:50 CPH:SA (12)). Polymer solubility changes due to the presence of anti-solvent caused spontaneous particle formation. These particles were removed from the anti-solvent by filtration (by aspiration using a Buechner funnel and Whatman #2 filter paper) and then dried overnight under vacuum. The procedure yielded a fine powder with at least 70% recovery. The nanosphere morphology was investigated using scanning electron microscopy (JEOL 840A, JEOL Ltd., Tokyo, Japan). Particle diameter was determined using quasi-elastic light scattering (Zetasizer Nano, Malvern Instruments Ltd., Worcester, UK).

Culture of THP-1 Human Monocytes and Co-Incubation with Nanospheres

Tissue culture and subsequent derivation of adherent THP-1 monocytes was performed according to published reports (34) with some modification (35). Briefly, THP-1 cells were grown in suspension using RPMI 1640 growth medium supplemented with 10% newborn calf serum, 10 mM Glutamax, 25 mM HEPES, and 10 μg/ml penicillin–streptomycin antibiotics (complete RPMI). Adherent monocytes were derived from suspension cultures by stimulating cells with 5 nM phorbol-12-myristic-13-acetate (PMA) in 24 well tissue culture plates containing 10 mm glass coverslips inside each well at a final density of 5×10^{5} cells per well. Following 24 h PMA incubation, cultures were washed with PBS and incubated in fresh RPMI without PMA for 24 h before nanospheres were added.

Polyanhydride nanospheres (in the form of dry powder) of poly(SA), 20:80 CPH:SA, or 50:50 CPH:SA were weighed and added to PBS (pH 7.4) at a stock concentration of 10 mg/ml. The nanospheres were briefly sonicated on ice for a total process time of 1 min alternating 10 sec pulse ON, 15 sec Pulse OFF. Nanospheres (100 μg) were added to cell culture medium (0.5 ml/well), briefly mixed by pipetting before cultures were returned to the incubator (37°C, 5% CO_2). In order to evaluate phagocytic processes, the nanospheres were co-incubated with the THP-1 cells for 30 min. Cultures were washed and the cells were placed back in the incubator for 2 h prior to analysis. In

order to evaluate endocytic processes, the nanospheres were co-incubated with the THP-1 cells for 6 h. Cultures were washed and the cells were placed back in the incubator for 48 h prior to analysis.

Fluorescence Microscopy Techniques

To observe time-dependent interactions of individual monocytes with nanospheres, cell monolayers incubated with nanospheres at indicated times were fixed with 4% paraformaldehyde (PFA) for 10 min at room temperature, and then washed with PBS. Acidic vesicles and lipid rafts in cell monolayers were labeled by incubating cells for 20 min prior to fixation with either Lysotracker at 1/2,000 dilution (DND-99)(acidic vesicles) or Alexa555 conjugated Cholera Toxin β-subunit (CTx) at 1/150 dilution (lipid rafts) (Molecular Probes-Invitrogen, Carlsbad, CA). Intracellular structures were immunofluorescently stained by incubating fixed coverslips with primary and secondary antibodies in PBS containing albumin and 0.1% saponin (BSP) (35). Stained coverslips were washed and mounted on glass slides (Pro-Long w/ Dapi; Molecular Probes-Invitrogen). Epifluorescence and immunofluorescence microscopy was performed using either an Olympus IX-61 inverted microscope equipped with blue, green, and red filter sets with a cooled CCD camera or by an inverted Leica NTS laser scanning confocal microscopy (LSCM). The LSCM is equipped with ApoChromatic ×63 oil and ×100 oil objectives and UV, Argon, Krypton and HeNe laser lines equipped with three photomultiplier detection tubes. Optimal step size for Z-stack image data was determined empirically from pilot studies to be 0.3 μm (data not shown). Co-localization analysis, relative nanosphere uptake comparisons, and final images were prepared using Image J v1.36b image analysis software loaded with particle counting algorithms (36).

Eα–RFP Antigen Preparation and Cellular Internalization by Monocytes

The IPTG inducible Eα–RFP expression construct was a kind gift from Dr. Marc Jenkins (Department of Microbiology, Center for Immunology, University of Minnesota Medical School (37) and introduced into *Escherichia coli* DH5α by heat shock followed by selecting 50 mg/ml ampicillin-resistant colonies. Broth cultures of transformed bacteria were induced by the addition of IPTG to overnight cultures. Crude cell lysates prepared using the Novagen Bugbuster extraction reagent (Gibbstown, NJ) were passed through a Profinity IMAC Ni-charged resin (BioRad; Hercules, CA). Imidazole eluted Eα–RFP protein was dialyzed overnight at 4°C and final preparations were shown to be free of detectable LPS contamination by the limulus ameobocyte lysate (LAL) assay (Cambrex; Walkersville, MD, USA). Fluorescence signal intensity of internalized protein was detected using standard epi-fluorescence microscopy employing TRITC/rhodamine filter set with 510–560 nm excitation and 575–645 emission. Image black levels for the RFP protein were set using cells not incubated with RFP. Exposure times for RFP detection were kept constant throughout the experimental groups to facilitate accurate comparative analysis. Bar graphs of the relative pixel intensity of internalized RFP were calculated from RAW-RFP images using the ImageJ/plugin/histogram function. These bar graphs reveal the relative pixel intensity of the RFP protein detected in the presence and absence of nanospheres.

RESULTS AND DISCUSSION

Nanosphere Characterization

Scanning electron photomicrographs of the FITC-dextran loaded nanospheres of varying formulations are presented in Fig. 2. The photomicrographs show that the nanoparticles appear circular, and while there are some small variations, the nanospheres appear to be relatively uniform in size and shape. Light scattering size distribution data show nanosphere diameters for all polymers fall between 200 and 800 nm.

Every batch of nanospheres was analyzed by light scattering and particle size was measured using duplicate samples. For each chemistry, the data from three different lots of nanospheres were analyzed in this manner and the compiled data are shown in Table I. The standard deviations were determined for the overall accumulated size distribution data for each polymer.

Analysis shows that there is no statistically significant difference in average particle size among the different polymer formulations ($p=0.13$). This data demonstrates that polyanhydride nanospheres fabricated by the PAN method can be reproducibly prepared with similar morphology and particle diameters regardless of copolymer chemistry. Having particles of similar size is important in limiting the variables that are introduced into *in vitro* and *in vivo* experiments, especially when evaluating a chemistry effect. While not statistically significant, there was a slight trend for a positive correlation between particle size and CPH content. The thermodynamic and kinetic balance between nucleation and growth dictates the resulting average particle size. The soluble material must nucleate particles and then more

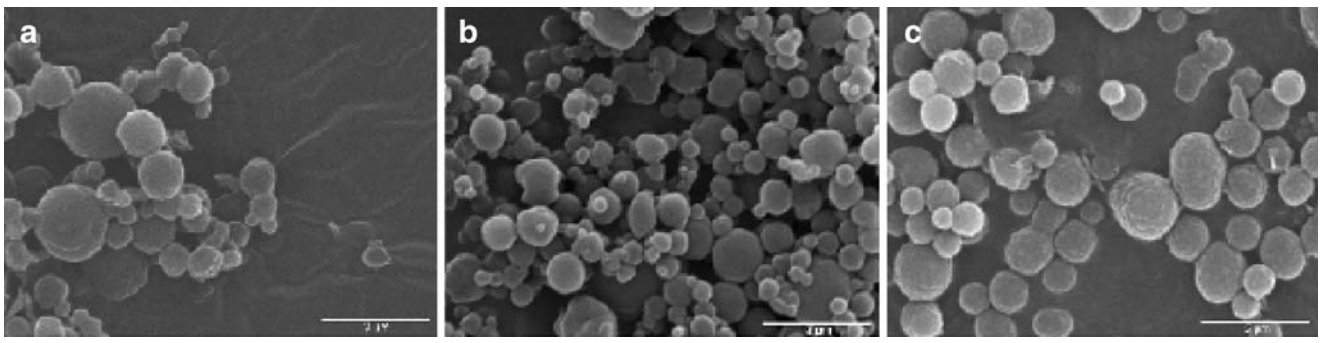

Fig. 2. Scanning electron photomicrographs of **a** poly(SA) nanospheres, **b** 20:80 CPH:SA nanospheres and **c** 50:50 CPH:SA nanospheres.

Table I. Particle Size Data Compiled from Light Scattering Measurements ($n=3$)

Polymer	Average Particle Diameter (nm)
poly SA	283±45
20:80 CPH:SA	348±48
50:50 CPH:SA	397±121

Data reported as mean±SD

material can either precipitate on the surface of these already formed particles or new particles can be nucleated (38). Copolymers with a higher SA content are less hydrophobic and more non-polar than those with a higher CPH content. When precipitating from a polar solvent into an aliphatic anti-solvent bath, copolymers with a higher SA content may more easily nucleate new particles. If nucleation is favored, it would cause more particles to be formed with a smaller average particle size.

Cellular Interactions of Nanospheres with Human Monocytes

To determine whether or not polymer chemistry affects nanoparticle internalization and intracellular deposition within APCs, adherent human THP-1 monocytes were incubated separately with poly(SA), 20:80 CPH:SA, or 50:50 CPH:SA nanospheres. LSCM was utilized to evaluate and compare the interactions of nanospheres with cells and their eventual intracellular localization.

Internalization

Nanospheres introduced into cell culture medium did not form large aggregates and remained uniformly dispersed prior to settling at the bottom of the tissue culture well during co-incubation with the THP-1 cells. The nanospheres were then rapidly internalized by THP-1 monocytes via cellular events consistent with phagocytosis (Fig. 3). Observations supporting this conclusion include: centrifugation-independent internaliza-

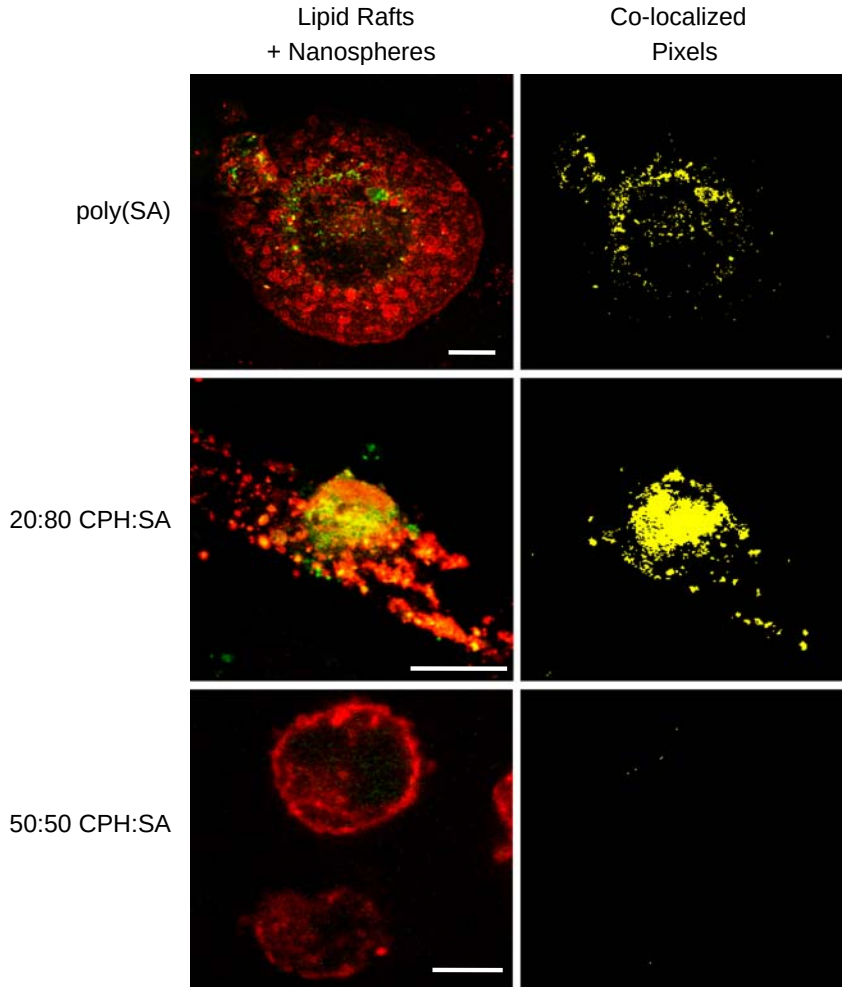

Fig. 3. Confocal photomicrographs of FITC-labeled polyanhydride nanospheres internalized by THP-1 cells. Adherent monocytes were incubated with nanospheres for 30 min before cultures were washed and continued to incubate for an additional 2 h. Poly(SA) and 20:80 CPH:SA nanoparticles were internalized to a much greater extent than 50:50 CPH:SA nanospheres. The majority of internalized poly(SA) and 20:80 CPH:SA were bound by cholesterol rich membranes as indicated by the high degree of co-localization (*yellow*). Representative images were captured by LSCM. Lipid rafts (*red*) were identified using Alexa 555 CTx (Molecular Probes). Scale bar=5 μm.

Table II. Association of Polyanhydride Nanospheres with THP-1 Cells Varies Depending on Polymer Chemistry

	Percent monocytes with internalized nanospheres[a]	
Polymer	2 h (phagocytosis)	48 h (phagocytosis and endocytosis)
Poly(SA)	87.9% ± 17.1%	96.3% ± 11.7%
20:80 CPH:SA	27.1% ± 14.8%	91.2% ± 22.2%
50:50 CPH:SA	8.1% ± 10.6%	53.1% ± 28.3

[a] Average percent nanospheres positive monocytes calculated per ×100 field of view image

tion, temperature-dependent internalization, and internalization in the absence of an overabundance of extracellular particles. Confocal photomicrographs in Fig. 3 depict monocytes that have internalized nanospheres and values presented in Table II indicate the percentage of THP-1 cells per field of view that have cell associated nanospheres at 2 or 48 h post exposure. Cells were imaged at 1000× total magnification and the average number of cells in each Field of View (FOV) was 25. FOVs were randomly selected and the numbers of THP-1 cells with FITC-loaded polyanhydride nanospheres or without nanospheres were recorded. The percentages and standard deviations of THP-1 cells positive for nanospheres were calculated from values for ≥5 FOV images for each nanosphere chemistry and time point (cells with FITC-nanospheres/total # cells scored). The total cells scored positively for clear association with FITC nanospheres were combined from data collected over three to five independent experiments. The data in Table II indicate that in the experiments designed to evaluate phagocytosis where the exposure to nanospheres was 30 min, the least hydrophobic polymers (i.e., poly(SA))

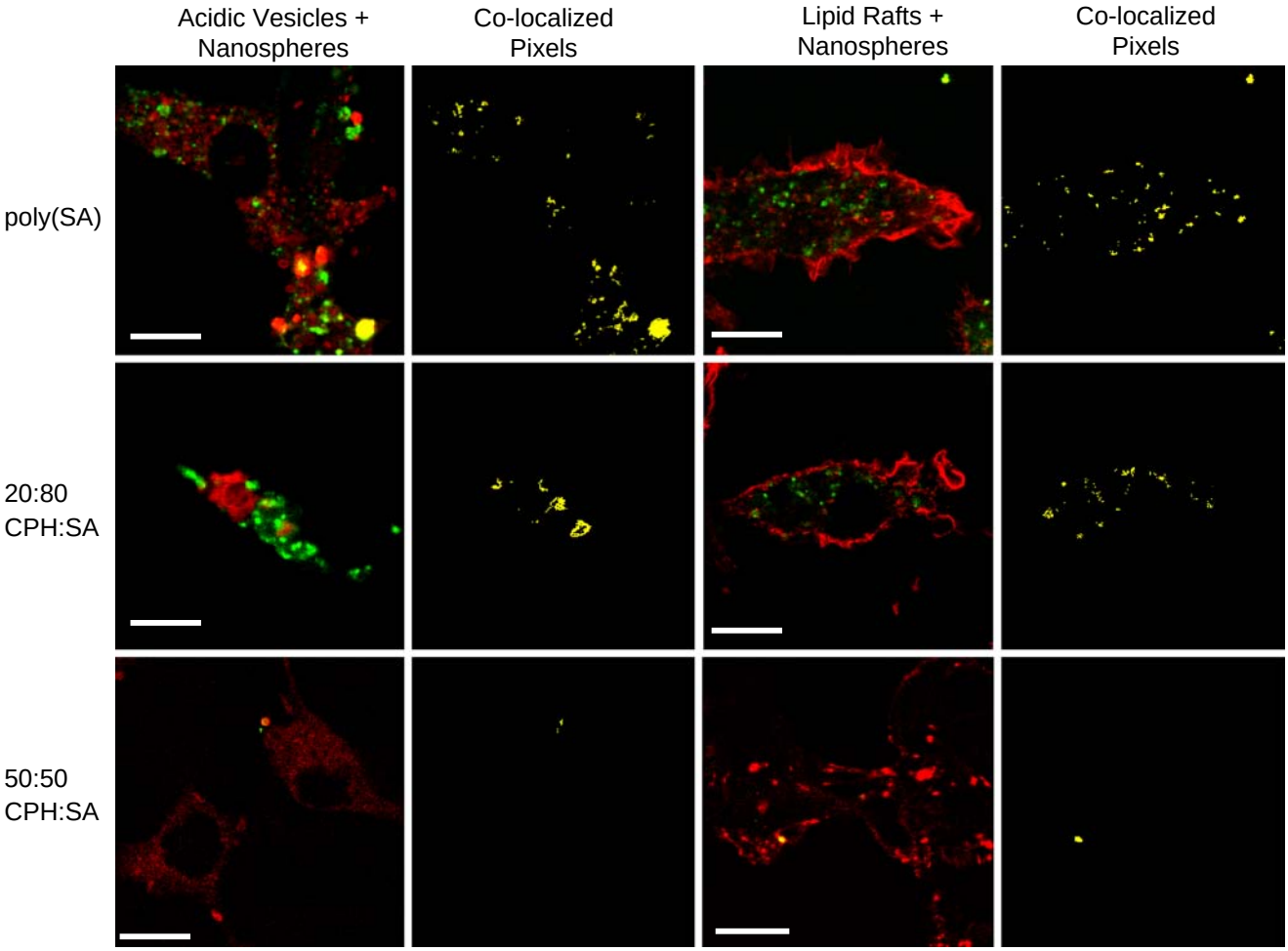

Fig. 4. Confocal images of the intracellular localization of FITC-nanospheres in THP-1 cells 48 h after uptake. Representative images were captured by LSCM and processed using ImageJ. The majority of internalized poly(SA) and 20:80 CPH:SA nanospheres were bound by cholesterol rich membranes as indicated by the high degree of co-localization (*yellow*). Acidic vesicles (*two left columns*) were identified using the pH responsive Lysotracker dye (*red*) and cholesterol rich lipid rafts (*two right columns*) were visualized using Alexa 555 conjugated CTx (*red*, Molecular Probes). Note the general absence of FITC 50:50 CPH:SA nanospheres compared to 20:80 CPH:SA and poly(SA). Scale bar=5 μm.

were more rapidly internalized than the more hydrophobic (i.e., CPH-containing) polymers (Fig. 3). In contrast, the 48 h co-localization experiments employ a longer exposure time of nanospheres with cells lasting 6 h. In these experiments, where endocytosis plus the initial phagocytosis would contribute to total nanosphere uptake, it was observed that ~96% of the THP-1 cells contained poly(SA) nanospheres, while the uptake of 20:80 CPH:SA and 50:50 CPH:SA was ~91% and ~53%, respectively. These results indicate that the chemistry of the polyanhydride nanospheres affects the uptake efficiency of these nanospheres by monocytes. Unlike CPH-containing nanospheres, poly(SA) nanospheres were more efficiently internalized by phagocytic processes (30 min exposure to cells) and did not require the extended time (6 h) associated with endocytic processes. The more hydrophobic nanospheres (i.e., CPH-rich) were not internalized by phagocytic pathways (~8%). However, with time, all the formulations were internalized; but, 50:50 CPH:SA nanospheres were internalized to a lesser extent (~53%, Table II). Overall, monocyte uptake of polyanhydride nanospheres correlated with decreasing hydrophobicity (poly(SA) > 20:80 CPH:SA > 50:50 CPH:SA).

The degree of hydrophobicity may indeed be an important factor influencing nanosphere uptake. The hydrophobic nature of these particles may facilitate their interaction with hydrophobic lipid-rich micro-domains in the cell membrane, including lipid rafts. Lipid rafts contain many membrane-bound cofactors that comprise receptor complexes, such as receptors for complement, antibodies, and serum and extracellular matrix proteins (39–41). In contrast with phagocytosis, increasing polymer hydrophobicity may facilitate closer nanosphere-to-cell interactions and increase the probability of internalization through constitutive endocytic or macropinocytotic pathways. These hydrophobic interactions facilitate nanosphere internalization by direct association with surface receptors or through direct interactions with the plasma membrane. Pattern recognition receptors (PRRs) are another key receptor type found in lipid rafts of APCs. PRRs recognize pathogen-associated molecular patterns (PAMPs), which are repetitive patterns of molecular structure found in both microorganisms and the mammalian host. Examples of PAMPs include lipopolysaccharide and flagellin from bacteria as well as hyaluronan and uric acid

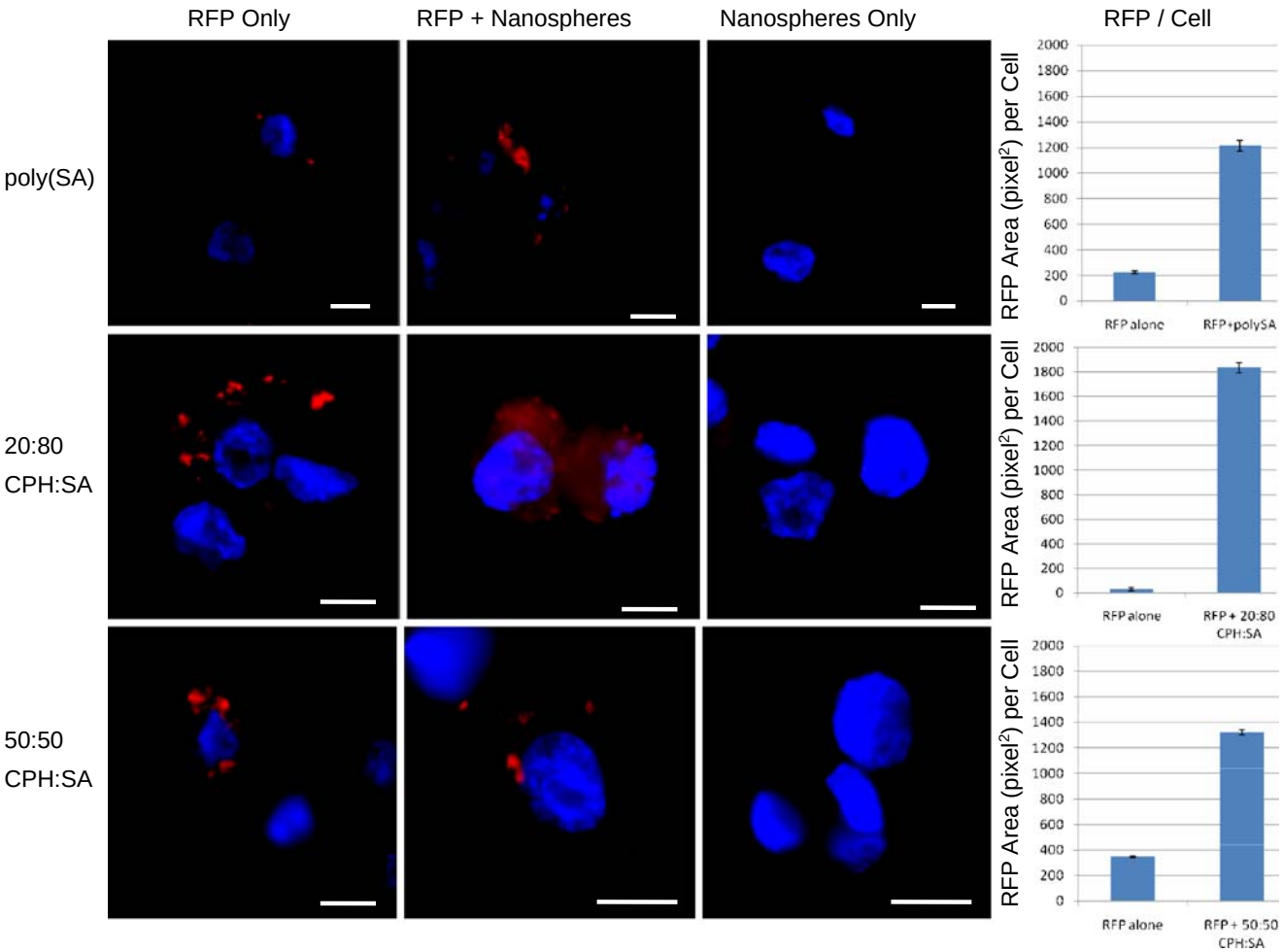

Fig. 5. Enhanced uptake of soluble Eα-RFP (*red*) antigen by monocytes (*nuclei blue*) after co-incubation with polyanhydride nanospheres for 2 h. Data demonstrated that the poly(SA) nanospheres enhanced antigen internalization more readily than did 20:80 CPH:SA followed by 50:50 CPH:SA. Representative epifluorescent images were captured and processed using identical exposure and ImageJ settings. *Adjacent bar graphs* summarize the average amount of RFP detected per cell. Pixel areas within each image correspond to relative intensity of RFP signal detected inside cells. Values from *three* randomly selected fields of view were used to calculate averages and SD. Scale bar=5 μm.

from mammals. All of these PAMPs signal "danger" to the host, be it in the context of infection or cellular damage. Hydrophobic characteristics have been ascribed to many PAMPs and are thought to be partly responsible for their immunostimulatory properties (42). In the context of the polyanhydride co-polymers, surface patterns of intervening hydrophobic moieties (e.g., CPH and SA, Fig. 1) may mimic PAMPs, facilitate interactions with PRRs present on the surface of APCs and subsequently enhance the ability of APCs to activate T cells (43, 44). Internalization and co-localization of antigen-loaded nanospheres within the endocytic pathway may, in part, explain the adjuvanticity of polyanhydride nanospheres (22).

Intracellular Localization

In general, intracellular degradation and processing of exogenously presented antigen occurs when lysosomes fuse with late endosomes containing antigen. In contrast, endogenous antigen is processed within the cytosol by the proteosome (45). As a result, antigen fate (i.e., MHC I *vs* MHC II presentation) is largely decided by intracellular location. Given the variable surface chemistry presented by the different polyanhydrides, we compared the intracellular distribution of nanospheres 48 h after uptake. The majority of particles were found to be intact and located within membrane bound vesicles that were characterized as acidic and CTx^+ (Fig. 4). In these photomicrographs, the FITC-dextran containing nanospheres appear green, the acidic vesicles are red (Lysotracker), and co-localized nanospheres within acidic vesicles appear yellow. The data indicates that all the polyanhydride chemistries studied resulted in localization of the nanospheres into the acidic phagolysosomal compartments of the cells.

The majority of these particles were rapidly targeted to the endosomal pathway, and localized within vesicles exhibiting staining characteristics and morphology consistent with MHC class II loading compartments (46). Interestingly, at 48 h, ~10% of the poly(SA) and 20:80 CPH:SA nanospheres did not appear to be located within acidic or lipid raft containing vesicles (Fig. 4). A lack of localization within either of these major intracellular compartments is consistent with nanospheres that are free within the cellular cytosol. Release of antigen from nanospheres located within the cellular cytosol would be processed and directed to the MHC class I presentation pathway (45). However, the data presented in Figs. 3 and 4 would only suggest that small amounts of nanospheres can reach the cytosol and that further experiments are warranted.

Antigen Internalization

As previously discussed, polyanhydride nanospheres serve as antigen delivery platforms to APCs. Nanosphere-encapsulated immunogens would be released intracellularly following internalization and slow polymer degradation (8). However, some nanospheres may release antigen prior to uptake, providing a source of soluble antigen delivered to APCs via endocytosis. To evaluate the ability of nanospheres to stimulate soluble antigen internalization by APCs, the THP-1 cells were co-incubated with blank nanospheres (poly (SA), 20:80 CPH:SA, or 50:50 CPH:SA) and soluble Eα–RFP (37), fixed, and visualized by epifluorescence microscopy. Representative photomicrographs and bar graphs summarizing cell associated RFP data are provided in Fig. 5. Comparisons among the three chemistries reveal that after 2 h of co-incubation, all three chemistries dramatically increased the amount of soluble antigen internalized by monocytes. A potential mechanism for the increase in uptake stimulated by the nanospheres is that the protein itself is able to adsorb on the surface of nanospheres that are then subsequently internalized by the APC. However, preliminary experiments failed to detect soluble RFP adsorbing onto FITC-labeled nanospheres (data not shown) and culture conditions include ample amounts of serum proteins present in the 10% fetal bovine serum supplemented medium. Moreover, the dramatic increase in the uptake of soluble RFP was also detected for 50:50 CPH:SA even though these particles serve as poor targets for uptake themselves (Table II, Figs. 3 and 4). This data demonstrates that the chemistry of the polyanhydride nanospheres influences the ability of APCs to internalize soluble antigen.

CONCLUSIONS

The unique cellular interactions elicited by polyanhydride nanospheres are a function of the particles' distinct physical and chemical properties that modulate the persistence and intracellular distribution of antigen. We observed that polyanhydride nanospheres were internalized and distributed within human monocytes in a chemistry-dependent manner. We also found that chemistry influences the ability of nanospheres to enhance monocytic uptake of soluble antigen. Together, this data highlights the importance of chemistry in designing polyanhydride nanospheres as vaccine or drug delivery vehicles intended for specific applications and/or targeting desired intracellular locations.

ACKNOWLEDGMENTS

B.N. and M.J.W. acknowledge financial support from the US Department of Defense—Office of Naval Research (ONR Award no. N00014-06-1-1176) and the Grow Iowa Values Fund. B.H.B. acknowledges startup funds provided by Iowa State University-College of Veterinary Medicine and the Office of Biotechnology. B.D.U acknowledges financial support from the Aileen S. Andrew Foundation. The authors acknowledge useful discussions with Dr. Amanda Ramer-Tait and Jenny Wilson-Welder. B.N. dedicates this work to Nicholas A. Peppas on the wonderful occasion of his sixtieth birthday.

REFERENCES

1. I. Preis, and R. S. Langer. A single-step immunization by sustained antigen release. *J. Immunol. Methods*. **28**(1–2):193–197 (1979) doi:10.1016/0022-1759(79)90341-7.
2. J. H. Wilson-Welder *et al.* Vaccine adjuvants: Current challenges and future approaches. *J. Pharm. Sci.* 2008.
3. S. P. Schwendeman. Recent advances in the stabilization of proteins encapsulated in injectable PLGA delivery systems. *Crit. Rev. Ther. Drug Carr. Syst.* **19**:73–98 (2002) doi:10.1615/CritRevTherDrugCarrierSyst.v19.i1.20.

4. A. Gopferich. Polymer bulk erosion. *Macromolecules*. **30**:2598–2604 (1997) doi:10.1021/ma961627y.
5. Y. Wang *et al.* Controlled release of ethacrynic acid from poly (lactide-co-glycolide) films for glaucoma treatment. *Biomaterials*. **25**(18):4279–4285 (2004) doi:10.1016/j.biomaterials.2003.10.075.
6. K. Fu *et al.* Visual evidence of acidic environment within degrading poly(lactic-co-glycolic acid) (PLGA) microspheres. *Pharm. Res*. **17**(1):100–106 (2000) doi:10.1023/A:1007582911958.
7. A. G. Ding, and S. P. Schwendeman. Acidic microclimate pH distribution in PLGA microspheres monitored by confocal laser scanning microscopy. *Pharm. Res*. **25**(9):2041–2052 (2008) doi:10.1007/s11095-008-9594-3.
8. A. S. Determan *et al.* Protein stability in the presence of polymer degradation products: consequences for controlled release formulations. *Biomaterials*. **27**(17):3312–3320 (2006) doi:10.1016/j.biomaterials.2006.01.054.
9. A. S. Determan *et al.* Encapsulation, stabilization, and release of BSA-FITC from polyanhydride microspheres. *J. Control. Release*. **100**(1):97–109 (2004) doi:10.1016/j.jconrel.2004.08.006.
10. G. Zhu, S. R. Mallery, and S. P. Schwendeman. Stabilization of proteins encapsulated in injectable poly(lactic-co-glycolic acid). *Nat. Biotechnol*. **18**:52–57 (2000) doi:10.1038/71916.
11. M. J. Kipper *et al.* Design of an injectable system based on bioerodible polyanhydride microspheres for sustained drug delivery. *Biomaterials*. **23**(22):4405–4412 (2002) doi:10.1016/S0142-9612(02)00181-3.
12. E. Shen *et al.* Mechanistic relationships between polymer microstructure and drug release kinetics in bioerodible polyanhydrides. *J. Control. Release*. **82**(1):115–125 (2002) doi:10.1016/S0168-3659(02)00125-6.
13. E. Ron *et al.* Controlled release of polypeptides from polyanhydrides. *Proc. Natl. Acad. Sci. USA*. **90**(9):4176–4180 (1993) doi:10.1073/pnas.90.9.4176.
14. L. Shieh *et al.* Erosion of a new family of biodegradable polyanhydrides. *J. Biomed. Materi. Res*. **28**(12):1465–1475 (1994) doi:10.1002/jbm.820281212.
15. J. P. Jain *et al.* Role of polyanhydrides as localized drug carriers. *J. Control. Release*. **103**(3):541–563 (2005) doi:10.1016/j.jconrel.2004.12.021.
16. A. S. Determan *et al.* The role of microsphere fabrication methods on the stability and release kinetics of ovalbumin encapsulated in polyanhydride microspheres. *J. Microencapsul*. **23**(8):832–843 (2006) doi:10.1080/02652040601033841.
17. Y. Tabata, S. Gutta, and R. Langer. Controlled delivery systems for proteins using polyanhydride microspheres. *Pharm. Res*. **10**(4):487–496 (1993) doi:10.1023/A:1018929531410.
18. B. A. Pfeifer *et al.* Poly(ester-anhydride):poly(beta-amino ester) microspheres and nanospheres: DNA encapsulation and cellular transfection. *Int. J. Pharm*. **304**(1–2):210–219 (2005) doi:10.1016/j.ijpharm.2005.08.001.
19. N. B. Shelke, and T. M. Aminabhavi. Synthesis and characterization of novel poly(sebacic anhydride-co-Pluronic F68/F127) biopolymeric microspheres for the controlled release of nifedipine. *Int. J. Pharm*. **345**(1–2):51–58 (2007) doi:10.1016/j.ijpharm.2007.05.036.
20. W. Hsu *et al.* Local delivery of interleukin-2 and adriamycin is synergistic in the treatment of experimental malignant glioma. *J. Neurooncol*. **74**(2):135–140 (2005) doi:10.1007/s11060-004-6597-8.
21. J. Hanes, M. Chiba, and R. Langer. Degradation of porous poly (anhydride-co-imide) microspheres and implications for controlled macromolecule delivery. *Biomaterials*. **19**(1–3):163–172 (1998) doi:10.1016/S0142-9612(97)00221-4.
22. M. J. Kipper *et al.* Single dose vaccine based on biodegradable polyanhydride microspheres can modulate immune response mechanism. *J. Biomed. Materi. Res. Part A*. **76**(4):798–810 (2006) doi:10.1002/jbm.a.30545.
23. C. Berkland *et al.* Microsphere size, precipitation kinetics and drug distribution control drug release from biodegradable polyanhydride microspheres. *J. Control. Release*. **94**(1):129–141 (2004) doi:10.1016/j.jconrel.2003.09.011.
24. F. X. Lacasse *et al.* Influence of surface properties at biodegradable microsphere surfaces: effects on plasma protein adsorption and phagocytosis. *Pharm. Res*. **15**(2):312–317 (1998) doi:10.1023/A:1011935222652.
25. J. A. Schwab, and M. Zenkel. Filtration of particulates in the human nose. *Laryngoscope*. **108**(1):120–124 (1998) doi:10.1097/00005537-199801000-00023.
26. P. A. Jaques, and C. S. Kim. Measurement of total lung deposition of inhaled ultrafine particles in healthy men and women. *Inhal. Toxicol*. **12**(8):715–731 (2000) doi:10.1080/08958370050085156.
27. M. P. Desai *et al.* Gastrointestinal uptake of biodegradable microparticles: effect of particle size. *Pharm. Res*. **13**(12):1838–1845 (1996) doi:10.1023/A:1016085108889.
28. T. Jung *et al.* Tetanus toxoid loaded nanoparticles from sulfobutylated poly(vinyl alcohol)-gradt-poly(lactide-co-glycolide): evaluation of antibody response after oral and nasal application in mice. *Pharm. Res*. **18**(3):352–360 (2001) doi:10.1023/A:1011063232257.
29. L. Illum. Nanoparticulate systems for nasal delivery of drugs: a real improvement over simple systems? *J. Pharm. Sci*. **96**(3):473–483 (2007) doi:10.1002/jps.20718.
30. M. P. Desai *et al.* The mechanism of uptake of biodegradable microparticles in Caco-2 cells is size dependent. *Pharm. Res*. **14**(11):1568–1573 (1997) doi:10.1023/A:1012126301290.
31. J. E. Fuller *et al.* Intracellular delivery of core-shell fluorescent silica nanoparticles. *Biomaterials*. **29**(10):1526–1532 (2008) doi:10.1016/j.biomaterials.2007.11.025.
32. A. Conix. Poly[1,3-bis(p-carboxyphenoxy)propane anhydride]. *Macromolecular Synthesis*. 2:95–98 (1966).
33. E. Mathiowitz *et al.* Biologically erodible microspheres as potential oral drug delivery systems. *Nature*. **386**(6623):410–414 (1997) doi:10.1038/386410a0.
34. R. W. Stokes, and D. Doxsee. The receptor-mediated uptake, survival, replication, and drug sensitivity of *Mycobacterium tuberculosis* within the macrophage-like cell line THP-1: a comparison with human monocyte-derived macrophages. *Cell. Immunol*. **197**(1):1–9 (1999) doi:10.1006/cimm.1999.1554.
35. B. H. Bellaire, R. M. Roop II, and J. A. Cardelli. Opsonized virulent *Brucella abortus* replicates within nonacidic, endoplasmic reticulum-negative, LAMP-1-positive phagosomes in human monocytes. *Infecation and Immunity*. **73**(6):3702–3713 (2005) doi:10.1128/IAI.73.6.3702-3713.2005.
36. *ImageJ*. Image Processing and Analysis in Java [cited 2008 August 3rd]; Available from: http://rsb.info.nih.gov/ij/.
37. A. A. Itano *et al.* Distinct dendritic cell populations sequentially present antigen to CD4 T cells and stimulate different aspects of cell-mediated immunity. *Immunity*. **19**(1):47–57 (2003) doi:10.1016/S1074-7613(03)00175-4.
38. E. Mathiowitz, *et al.* Process for preparing microparticles through phase inversion phenomena. 2003: United States of America.
39. P. Lajoie, and I. R. Nabi. Regulation of raft-dependent endocytosis. *J. Cell. Mol. Med*. **11**(4):644–653 (2007) doi:10.1111/j.1582-4934.2007.00083.x.
40. N. Gupta, and A. L. DeFranco. Visualizing lipid raft dynamics and early signaling events during antigen receptor-mediated B-lymphocyte activation. *Mol. Biol. Cell*. **14**(2):432–444 (2003) doi:10.1091/mbc.02-05-0078.
41. Z. Wolf *et al.* Monocyte cholesterol homeostasis correlates with the presence of detergent resistant membrane microdomains. *Cytometry Part A*. **71**(7):486–494 (2007) doi:10.1002/cyto.a.20403.
42. S. Y. Seong, and P. Matzinger. Hydrophobicity: an ancient damage-associated molecular pattern that initiates innate immune responses. *Nat. Rev. Immunol*. **4**(6):469–478 (2004) doi:10.1038/nri1372.
43. M. G. Netea *et al.* From the Th1/Th2 paradigm towards a Toll-like receptor/T-helper bias. *Antimicrob. Agents Chemother*. **49**(10):3991–3996 (2005) doi:10.1128/AAC.49.10.3991-3996.2005.
44. P. Elamanchili *et al.* "Pathogen-mimicking" nanoparticles for vaccine delivery to dendritic cells. *J. Immunother*. **30**(4):378–395 (2007) doi:10.1097/CJI.0b013e31802cf3e3.
45. A. L. Goldberg *et al.* The importance of the proteasome and subsequent proteolytic steps in the generation of antigenic peptides. *Mol. Immunol*. **39**(3–4):147–164 (2002) doi:10.1016/S0161-5890(02)00098-6.
46. E. M. Hiltbold, and P. A. Roche. Trafficking of MHC class II molecules in the late secretory pathway. *Curr. Opin. Immunol*. **14**(1):30–35 (2002) doi:10.1016/S0952-7915(01)00295-3.